Journal of Oil Palm Research Vol. 37 (2) June 2025 p. 288-299
DOI: https://doi.org/10.21894/jopr.2024.0025

OBJECT-BASED IMAGE ANALYSIS (OBIA) ON HYPERSPECTRAL IMAGERY FROM DRONE FOR *Ganoderma* BASAL STEM ROT DISEASE DETECTION IN OIL PALM

MOHAMAD ANUAR IZZUDDIN[1]; AROF HAMZAH[2]*; MOHD NOOR NISFARIZA[3] and ABU SEMAN IDRIS[1]

ABSTRACT

Ganoderma *basal stem rot (BSR) disease infection in oil palm causes significant yield loss to the industry. An efficient disease control application is practical during early and moderate infection of* Ganoderma *in oil palm. Early detection of disease caused by* Ganoderma *has been conducted in the lab and on the ground manually. This approach requires inspection and sampling of each oil palm in the field, which is laborious, time-consuming, and costly. Airborne detection using a drone provides a good alternative for fast* Ganoderma *BSR disease detection in oil palms. This study uses hyperspectral images obtained from a camera mounted on a drone and Object-based Image Analysis (OBIA) to detect* Ganoderma *infection in oil palms and classify the* Ganoderma *BSR Disease Severity Index (GDSI). In OBIA, segmentation parameters, such as the Edge were set to 30 while Merge was set to 70 to demarcate respective oil palm without overlaps. Two classifiers namely 1) Support Vector Machine (SVM) and 2) K-Nearest Neighbour (KNN) were used to classify the segmented samples for each GDSI. The results demonstrate that the SVM classifier provides a good classification of the raster image with an overall accuracy of 92.5%. The study shows that hyperspectral images captured by drones provide a viable technique for detecting* Ganoderma *infection and classifying its severity.*

Keywords: drone, *Ganoderma*, hyperspectral, image segmentation.

Received: 1 August 2023**; Accepted:** 28 December 2023**; Published online:** 1 April 2024.

INTRODUCTION

The basal stem rot (BSR) disease caused by *Ganoderma boninense* has caused significant economic loss to oil palm plantations (Basiron, 2007; Roslan & Idris, 2012) ranging from 31% to 67% resulting in the decreased yield of fresh fruit bunches (FFB) from 26% to 45% which is a huge loss to oil palm planters (Singh, 1991). The indicator of the disease is the presence of basidiomata of the pathogen in the stem base or frond bases or the root (Idris *et al.,* 2004). The *Ganoderma* invades the oil palm through the root and spreads towards the bole and the stem base. Moderate and severe infection of *Ganoderma* BSR disease in the bole causes visual symptoms in the oil palm canopy (Flood *et al.,* 2022). The understanding of symptoms and physiological changes of oil palms after *Ganoderma* infection is important to develop a practical approach to detecting *Ganoderma* BSR infection as early as possible.

Several ground and lab-based technologies have been developed for detecting *Ganoderma* in oil palms, namely through the use of the *Ganoderma* Selective Medium (GSM) (Idris *et al.,* 2006); Polyclonal Antibodies Enzyme-Linked Immunosorbent Assay (PAbs-ELISA) (Idris & Rafidah, 2008) and GanoSken Tomography (Idris *et al.,* 2010; Mazliham *et al.,* 2006). These ground and lab-based detection

[1] Malaysian Palm Oil Board,
6, Persiaran Institusi, Bandar Baru Bangi,
43000 Kajang, Selangor, Malaysia.

[2] Department of Electrical Engineering,
Faculty of Engineering, University of Malaya,
50603 Kuala Lumpur, Malaysia.

[3] Department of Geography,
Faculty of Arts and Social Sciences,
University of Malaya,
50603 Kuala Lumpur, Malaysia.

* *Corresponding author e-mail: ahamzah@um.edu.my*

methods require inspecting and taking samples from individual oil palms in the field. They are costly, time-consuming, and laborious. Thus, there is a need for a more practical technology that can detect *Ganoderma* in oil palms rapidly and efficiently, suitable for a large area of oil palm plantation. Aerial-based detection of *Ganoderma* infection can assist plantation managers in monitoring the health status of many oil palms in the field without the need to inspect individual oil palms on the ground. This approach provides an effective way to control disease and conduct a viable rehabilitation programme.

Previously, the Malaysian Palm Oil Board (MPOB) in collaboration with the University of Malaya (UM) and Universiti Putra Malaysia (UPM) had conducted preliminary diagnostic studies on the application of ground-based remote sensing technologies or hyperspectral field spectroscopy for the detection of *Ganoderma* in oil palms (Izzuddin, 2010; Nisfariza, 2012; Shafri *et al.,* 2011). Following the success of the ground-based investigations, the efforts were expanded to airborne platforms using manned fixed-wing aircraft mounted with hyperspectral cameras which generated promising results. By analysing the data, *Ganoderma* infection was detected and classified into three classes of disease severity which are healthy, early infected and severely infected (Nisfariza, 2012). The work was then extended further using a lightweight drone mounted with a multispectral camera (Izzuddin *et al.*, 2018; 2020). However, there are challenges in the development of early detection techniques using hyperspectral images for the *Ganoderma* disease infection in oil palm due to the complexity of spatial and spectral properties of the hyperspectral image cube. The challenges are in developing a new procedure for colour-balancing of image mosaic, image transformation to enhance spectral properties, denoising to remove noise due to illumination and climate effects, and also selection of significant wavelengths that give higher spectral-separability between features (Izzuddin *et al.,* 2018; Liang, 2017; Nisfariza, 2012).

Thus, this study attempts to examine the capabilities of hyperspectral remote sensing images acquired from drones to detect *Ganoderma* infection in oil palms. Previous studies conducted using moderate spatial and spectral resolution multispectral and hyperspectral remote sensing showed that the healthy and early *Ganoderma* BSR infected oil palms were hard to discriminate due to similar canopy morphology and spectral signatures for both categories. The introduction of new and advanced upgrades of the Automated Orders and Resource System (AORS) that can be mounted on drones, which is more precise, smaller in size, durable, and provide higher spatial and spectral resolution images had given a new opportunity for further research for the detection of *Ganoderma* in oil palm. The high spatial and spectral resolution of the new generation multispectral and hyperspectral technologies also need new and advanced data classifier that can handle higher spectral dimensions of AORS imagery data.

Advanced imagery such as OBIA that integrate image segmentation analysis with an advanced classifier such as a Support Vector Machine (SVM) can increase classification accuracy for AORS images. Several studies on the application of these advanced classifiers for optical remote sensing images have shown remarkable accuracy of results. Therefore, this study was conducted to develop enhanced image analysis techniques based on these advanced data classifiers to discriminate between all levels of *Ganoderma* infection severity in oil palms.

MATERIALS AND METHODS

Figure 1 shows the flow of work involved in this study. The data are acquired from drone and ground census and both data were pre-processed to prepare the datasets for further processing using OBIA. Ground data was used for accuracy assessment of the classification results.

Area of Study

The study area was located in Lekir, Perak, Malaysia (4°12′3.43″N, 100°47′7.87″E). The area covers an estimated 30 ha and is planted with nine-year old commercial *Dura* x *Pisifera* (DxP) planting materials. The annual rainfall is 2,100 mm/yr. The area consisted of coastal soil which is the Sogomana-Setiawan series. The area only reported the presence of *Ganoderma*, and no other diseases, pests, or nutrient deficiencies have been reported.

Equipment and Devices

In this study, a hyperspectral drone was used for airborne image acquisition in September 2019. The hyperspectral drone system consisted of a RESONON Pika L hyperspectral camera (RESONON Inc., Montana, USA) mounted on a DJI M600 Pro hexacopter drone (*Figure 2*). The camera captured hyperspectral images consisting of image scanlines of 300 bands from 350-1,018 nm. The drone was flown at 80 m altitude to obtain a 10 cm spatial resolution hyperspectral image for each scanline. A calibration tarp was also laid on the open space near the study area during drone hyperspectral image acquisition. The gray tarp was used for image calibration during hyperspectral image radiometric correction. The image acquisition was conducted from 10:00 to 11:30 am on a sunny day, with a low amount of cloud cover (< 30%).

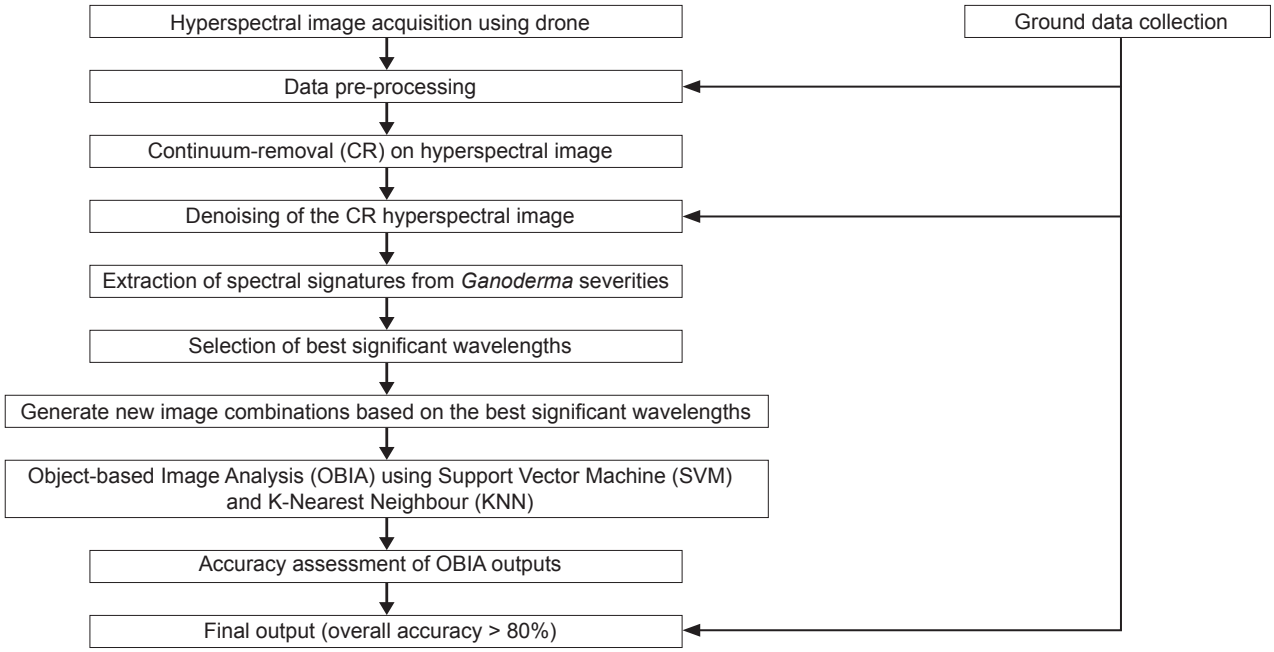

Figure 1. Flowchart of methodology.

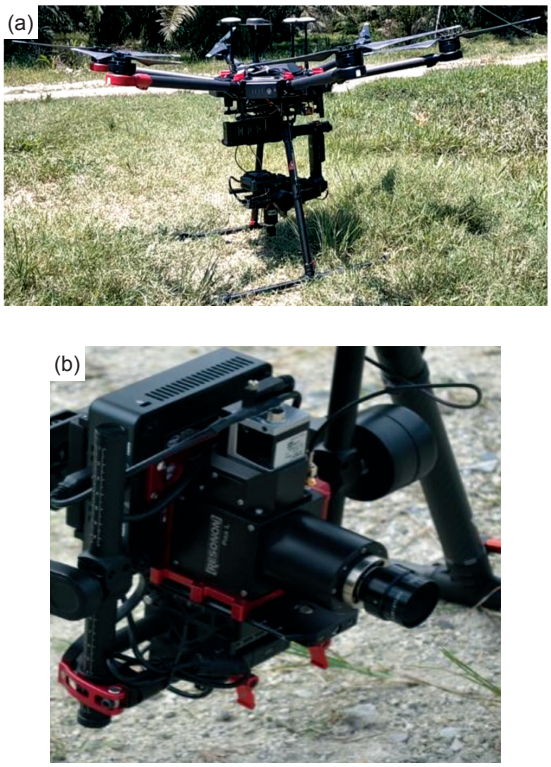

Figure 2. (a) The DJI M600 Pro hexacopter drone with hyperspectral camera and (b) RESONON Pika L camera.

The RESONON Pika L camera is linked to an Eclipse Inertial Measurement Unit (IMU) system that assisted in tagging each scanline recorded during flight to a defined coordinate system. The coordinate system used in this study is World Geodetic System 84 (WGS 84), Universal Transverse (UTM) Zone 47 North (N). The flight plan and image acquisition parameter settings were defined and set using RESONON Ground Station software while the drone navigation setting parameters were set using DJI GSPro software.

Ground Data Collection

The ground data collection was conducted during drone data acquisition. The ground data consisted of a ground census of the severity of the infection which is based on the *Ganoderma* Infection Severity Index (GDSI) mentioned in *Standard Operating Procedures (SOP) Guidelines for Managing* Ganoderma *Disease in Oil Palm* (Idris *et al.*, 2016) (*Table 1*). The ground census procedure is conducted by manual inspection of the base of the oil palm stem for the presence of *Ganoderma* basidiocarp, small white button, white mycelium, or rotting. Tissue samples are taken from the base stem using drilling techniques and then tested using the *Ganoderma* Selective Medium (GSM). Then, the severity of the infection was determined by inspection of the oil palm frond morphology.

Ground measurement of spectral signatures from healthy oil palm foliar was also conducted during the ground census. The spectral signatures were measured in the field using a portable spectroradiometer GER 1500 that recorded the spectral signatures from 350-1,050 nm. The spectral signatures were measured using a measurement probe with a leaf clipper attached to the spectroradiometer using a fibre optic cable. The probe was equipped with a halogen-lamp as a source of illumination. The leaf clipper has white calibration reference attached with the probe for calibration reference before each measurement was taken.

TABLE 1. *Ganoderma* BASAL STEM ROT DISEASE SEVERITY INDEX (GDSI)

Severity	0	1	2	3
	Description			
Category	Healthy	Early/Mild	Moderate	Severe
			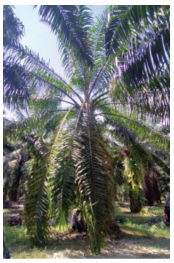	
0	No existence of *Ganoderma* fruiting bodies, no foliar symptoms, and no evidence of rotting at the base of the stem, negative results for GSM and PCR-DNA test.			
1	Existence of *Ganoderma* fruiting bodies or rotting or both at the base stem of oil palm and no foliar symptoms.			
2	Existence of white mycelia fruiting bodies of *Ganoderma* at the base of the stem, the existence of foliar symptoms such as yellowing and lowering of older fronds (<30%). Presence of rotting at the base of the stem (<30%), positive results for *Ganoderma* using GSM or PCR-DNA test.			
3	Existence of white mycelia fruiting bodies of *Ganoderma* at the base of the stem. Severe foliar symptoms (>30%) and rotting at the base of the stem (>30%), positive results for *Ganoderma* using GSM or PCR-DNA test.			

Data of Pre-processing and Denoising

The raw hyperspectral images were captured in the form of scanlines saved in *.bip* format. Each of the scanlines consisted of 300 bands. The scanlines were radiometrically and geometrically corrected using Spectronon Pro software to generate an orthorectified image (RESONON Inc., Montana, USA). Post correction, the best orthorectified scanlines with good visual were used as the reference image for mosaicking, generate orthomosaiced image and also colour balance correction processes using the mosaicking tool provided by ENVI 5.0 software. Meanwhile, ground census data were digitised into vector files containing the infection severity attributes of each oil palm using ArcGIS Pro software. The digitised data was saved in shapefile (*.shp*) format file.

Following that, the continuum-removal (CR) process was applied to the mosaiced hyperspectral image by dividing it into actual spectrum for each pixel in the image:

$$S_{cr} = (S/C) \quad (1)$$

where, S_{cr} is continuum-removed spectra, S is original spectrum and C is continuum curve.

The resulting image spectra equals to 1.0 is when the continuum and the spectra matches, and less than 1.0 when absorption features occur. The CR was used to normalise reflectance spectral to compare individual absorption features from a common baseline. Then, the CR hyperspectral image in spectral reflectance (SR) was converted into the first derivative of spectral reflectance (FDSR) image using the algorithm below.

The FDSR was generated using:

$$FD = \frac{y_2 - y_1}{x_2 - x_1} FD = \frac{y_2 - y_1}{x_2 - x_1} \quad (2)$$

where FD is the denoised first derivative that was computed with inputs y_2 and y_1 namely, the reflectance spectra at the second and first wavelengths. The values x_2 and x_1 represent the second and first wavelengths.

In this study, two types of hyperspectral imageries were prepared as input for denoising and analysis which are: 1) Denoised and continuum removed spectral reflectance image (D-CR SR) and 2) denoised and continuum-removed first derivative of spectral reflectance image (D-CR FDSR) was used in the selection for best significant wavelengths and then the OBIA was used for the image classification into the disease severities.

Denoising started with the manual removal of noisy bands. The process needs manual visual assessment on each of the image displays from each wavelength one-by-one. The ENVI 5.0 software was used to display the images in each discreet wavelength. Then, the image from wavelengths which showed a blurred appearance containing lots of speckles and noise that made it difficult to visually interpret oil palm canopies were removed from the hyperspectral image. The remaining bands that show a clear image of the oil palm canopies were retained for further denoising process using the Savitzky-Golay (S-G) denoising technique (Ruffin *et al.*, 2008). The best denoising settings were conducted using comparison with ground-based spectral signatures obtained from

TABLE 2. SAVITZKY-GOLAY (S-G) DENOISING PARAMETER SETTINGS

Set	Denoising parameters	1	2	3	4	5
A	Filter width	1	5	10	15	20
	Order of derivative	1	1	1	1	1
	Degree of polynomial	1	1	1	1	1
B	Filter width	1	5	10	15	20
	Order of derivative	1	1	1	1	1
	Degree of polynomial	2	2	2	2	2
C	Filter width	1	5	10	15	20
	Order of derivative	1	1	1	1	1
	Degree of polynomial	3	3	3	3	3

field spectroscopy (Izzudin *et al.*, 2013). The images were denoised using three different S-G denoising parameter settings which are the filter width and degree of polynomial, namely Set A, Set B and Set C (*Table 2*). The image denoising using S-G was conducted using ENVI 5.0 software.

Table 2 shows the 15 S-G denoising parameter settings that were used to denoise the CR hyperspectral image. The denoising parameters are Filter Width (FW), Order of Derivative (OD) and Degree of Polynomial (DoP). The best denoised image was chosen based on Root Mean Square Error (RMSE) and visual comparative analysis of denoised spectral signatures with the spectral signatures obtained from the ground-based field spectroscopy. The field spectroscopy used a field spectroradiometer to record spectral reflectance from the foliar of oil palm frond directly. In this study, a GER 1500 spectroradiometer is used to measure the spectral reflectance of a healthy oil palm foliar as the benchmark to select the best image denoising parameter.

Selection of Best Significant Wavelengths

The D-CR SR and D-CR FDSR hyperspectral images were overlaid with the ground census of GDSI vector file in ENVI 5.0 software to tag the oil palm canopies in the images with their respective GDSI. Then, the spectral signatures of the oil palm canopy were extracted from the fronds within 3 m radius from the middle of the canopy using ENVI 5.0 software. About 50 spectral signatures were extracted from each frond randomly selected on the oil palm canopy. The spectral signatures were extracted from 65/634 oil palms of GDSI 0, 35/51 oil palms of GDSI 1, 35/52 oil palms from GDSI 2 and 5/10 oil palms from GDSI 3. The number of oil palms for GDSI 2 and 3 is low because the incidence of moderate and severe *Ganoderma* disease is low in young to mature oil palms.

The number of healthy and early severity of the disease is adequate (>30 samples) for classification analysis using OBIA. The spectral signatures for each GDSI were stored in ASCII format (*.txt*). The spectral signatures from the bands for each D-CR SR and D-CR FDSR were analysed using Minimum Redundancy Maximum Relevance (MRMR) band by band to select the best 3, 5 and 7 significant wavelengths that can differentiate between all GDSI. The MRMR algorithm selects a subset of features having the most correlation with the class output and the least correlation between themselves. The algorithm ranks features according to minimal-redundancy-maximal-relevance criterion which is based on mutual information (Radovic *et al.*, 2017). The MRMR was conducted using MATLAB 2022a software. Then, the hyperspectral image from D-CR SR and D-CR FDSR were subset into 3, 5 and 7 best significant spectral bands image sets. The images were then used as input in OBIA.

Object-based Image Analysis (OBIA)

The OBIA comprises two major processes which are: 1) Segmentation and 2) classification. The first process is to select the best segmentation parameters that can demarcate a single oil palm canopy that does not overlap with adjacent trees in the image. The OBIA was conducted according to Izzuddin *et al.* (2020) and was made possible by the use of the watershed segmentation technique to segment the oil palm canopy to its respective canopy crown. The values are tested using a trial and error technique to select the best value combinations that reduce overlaps between oil palm canopy fronds.

In this analysis, the subset of hyperspectral images from 3, 5 and 7 best significant wavelengths are used as input for OBIA. The OBIA was conducted using ENVI 5.0 software. In this study, the best parameter settings that can segment the fronds of each canopy without overlapping into adjacent oil palm stands and visually provide differences at the edge between the oil palm canopy and the background were selected. The three best segments and merged parameters in this study are named Set 1, Set 2 and Set 3 with Edge chosen as segment settings, while the scale level is set to 20, 30 and 40

with merge settings at Full Lambda Schedule with respective merge level of 80, 70 and 60 and texture kernel size are set to 3. The scale and merge level are used to delineate features for detecting edges of features where objects of interest have sharp edges. The scale level delineates the boundaries of features as much as possible without over-segmenting the features. Increasing the scale value can generate fewer segments while decreasing the scale level value generates more segments. The merge level is used primarily to merge or combine segments with similar spectral information.

The workflow for this process involves multiple steps from preprocessing to segmentation, sample selection, training, classifying and accuracy assessment. Each step needs iteration with in-depth knowledge of the input imagery, classification schema, classification methods, expected results, and acceptable accuracy. The second process is a classification of the segmented image using: 1) OBIA with SVM and 2) OBIA with KNN.

The SVM classifier can process a segmented raster input or a standard image. It is less susceptible to noise, correlated bands and an unbalanced number or size of training sites within each class. The SVM usually use one of the four basic kernels which are linear, polynomial, sigmoid and radial basis functions (Gholami & Fakhari, 2017). The SVM has been used successfully in many data classification analyses with high accuracy (Azmi *et al.*, 2020). The SVM is a non-parametric classifier that requires a small sample size for training in the classification processes. This method is suitable for high-dimensional data with a limited training set (Cortes & Vapnik, 2015; Lan *et al.*, 2020). There are several parameter settings that need to be conducted to obtain the best classification model. The SVM hyperparameters input are: 1) Kernel scale; 2) kernel function; 3) box constraint level; 4) multiclass method and 5) standardised data. The SVM optimiser options are: 1) Optimiser; 2) acquisition function; 3) iterations and 4) training time limit.

Other than that, the KNN classifier computes the Euclidean distance from each segment in the segmentation image to every training region that is defined. The distance is measured in n-dimensional space, where n is the number of attributes for that training region. The classification process uses the area of attribute values and spectral mean attribute values and calculates the distance from the segment of training regions. In KNN, one parameter that needs to be set is the neighbour values that are comprised of odd values that depend on the number of total numbers of training regions for all classes. Other than that, the threshold value is set to 95% to indicate the level of confidence that the closest segments of any given segment represents the same class.

Accuracy Assessment

The accuracy of OBIA classification outputs of D-CR SR and D-CR FDSR were assessed using the percentage of correct classification over ground truth data. The method was also used by Izzuddin *et al.* (2020) to assess the accuracy of OBIA output for multispectral image analysis.

RESULTS AND DISCUSSION

Hyperspectral Orthomosaiced Image

The geometrically and radiometrically corrected hyperspectral image scanlines are orthomosaiced and colour-balanced using ENVI 5.0 software (*Figure 3*). The colour balance correction was conducted by selecting one reference image scanline that has uniform brightness and tone. The selection of the reference image scanline was conducted manually using visual eye inspection. Then, the statistics of max and min pixel values of the reference scanline are measured and the colour balance process was conducted using complete overlap scanline statistics for the mosaic image.

This section also consists of the results of the image denoising, selection of the best significant wavelengths, segmentation and classification of new images generated from the significant wavelengths and the accuracy of the classification into different degrees of *Ganoderma*-infection severity.

Hyperspectral Denoising

The results of spectral denoising of the hyperspectral image were selected based on comparison with the ground-based field spectroradiometer measurements of oil palm foliar on fronds. The comparison of ground-based spectroradiometer and the denoised spectral signatures is shown in *Figure 4*. The results showed that the S-G with Filter Width 5, Level of Derivative 1 and Degree of Polynomial 2 is the best denoised parameter setting to denoise the image.

Figure 4 shows the comparison of denoised spectral signatures from the hyperspectral image and clean spectral signatures measured using field spectroscopy in the field from healthy oil palm. The denoising outputs show that Set B2 give the best denoising results compared to Set C3 output visually not similar to the field spectroscopy spectral signature. The results showed that the denoised spectral signatures of hyperspectral using Set B2 have similar spectral signatures with the reference spectral signatures in terms of pattern and magnitude meanwhile denoising using Set C3 resulted in over denoising effect where the slope of the derivative seems to be a very smooth.

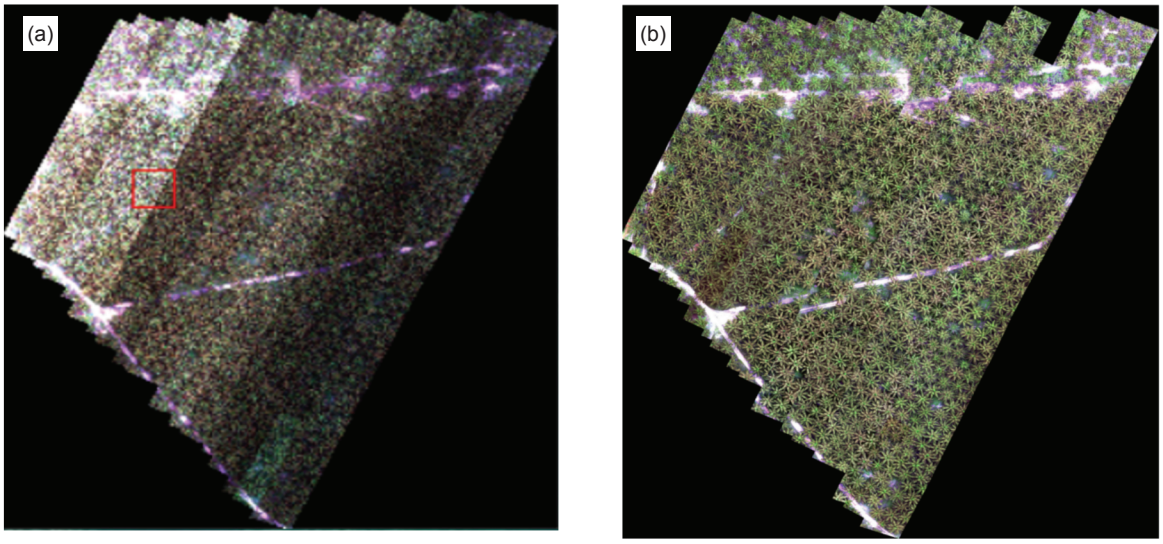

Figure 3. The geometrically and radiometrically corrected airborne hyperspectral image mosaic of the study area: (a) True colour (band combination: 35, 79 and 179 (450.10, 540.41 and 664.12 nm) before colour balance process and (b) true colour after colour balance process.

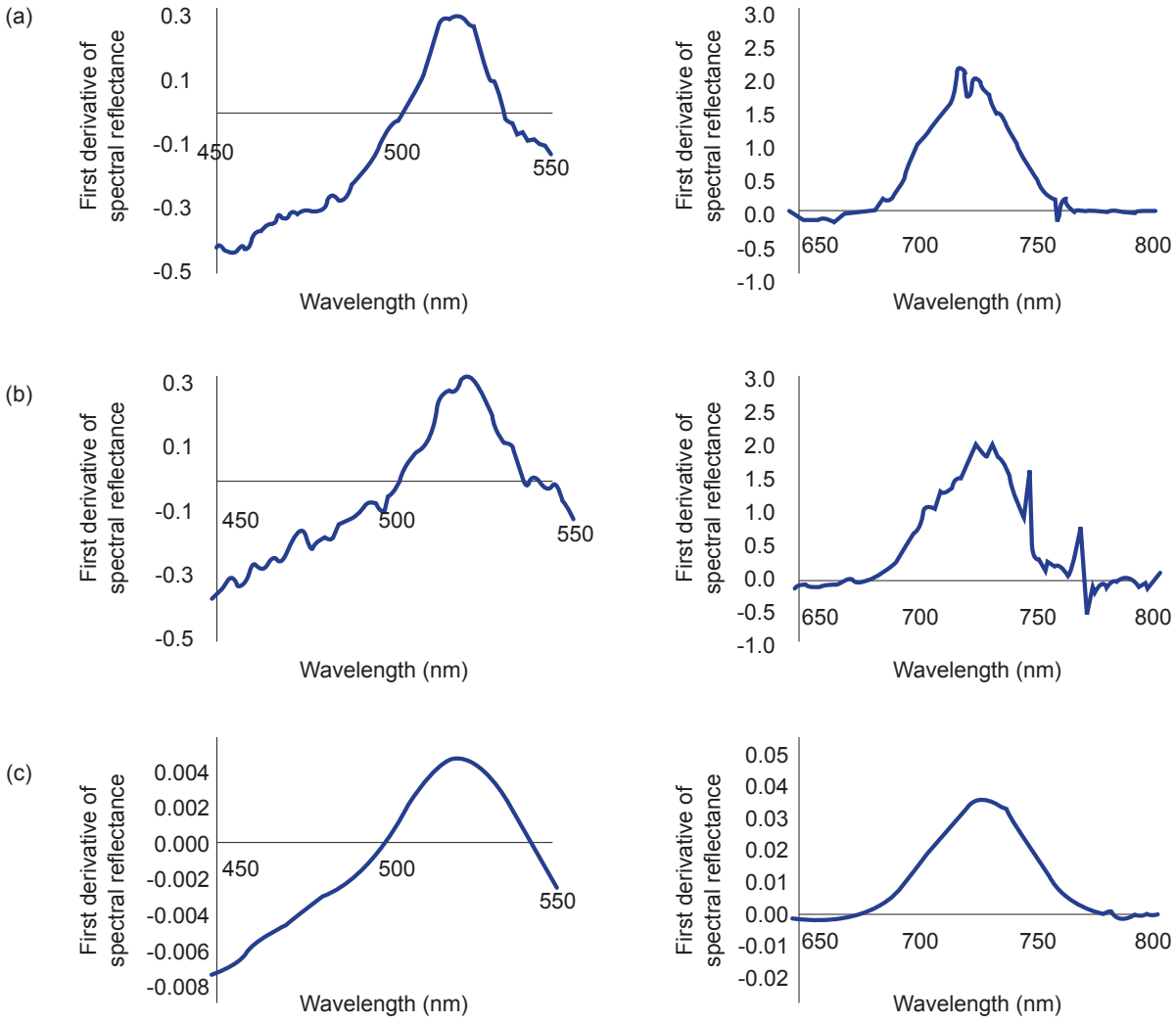

Figure 4. Spectral comparison between (a) clean first derivative spectral signature from field spectroscopy measurement while (b) the denoised first derivative of spectral signature from hyperspectral image using Set B2 and (c) using Set C3 from 450 to 550 nm and 650 to 800 nm.

The best denoising parameter settings were analysed using Root Mean Square Error (RMSE). Fifty-two wavelengths were chosen as sample points from the CR FDSR image for RMSE calculation. The 52 wavelengths comprised 10 wavelengths (401.70 to 417.11 nm), 10 wavelengths (531.48 to 547.75 nm), 10 wavelengths (654.26 to 668.66 nm), 10 wavelengths (732.22 to 746.41 nm), 10 wavelengths (850.63 to 864.46 nm) and 2 wavelengths (901.18 and 902.71 nm). The FDSR values from these wavelengths were used to calculate the RMSE. A larger RMSE value indicates worse denoising output. Smaller RMSE indicates better denoising output that is similar and fits with the reference spectral signatures from ground measurement. The results showed that the RMSE for Set B2 was 0.009934903 while the RMSE for Set C3 was 0.010271097 (*Table 3*).

For further processing, the denoised hyperspectral image was analysed to select the best 3, 5 and 7 significant wavelengths. In this study, MRMR technique was used on the D-CR-SR and D-CR-FDSR. *Table 4* shows the best 3, 5 and 7 significant wavelengths from D-CR-SR and D-CR-FDSR. Then, three new spectral subsets of hyperspectral image were generated using ENVI 5.0 software based on the 3, 5 and 7 best significant wavelengths. The best significant wavelengths were arranged according to their discriminatory capability index obtained from the MRMR analysis. The OBIA was conducted using ENVI 5.0 software. The Example-based Feature Extraction (EFE) tool was used to process and analyse the 3, 5 and 7 spectral subset hyperspectral image in ENVI 5.0.

In this study, three settings of image segmentation were used, and the best setting is Set 2 which used the value 30 for the segment and 70 for merging with Kernel value of 3. The segmentation process had segmented the fronds of the canopy with good separation between adjacent oil palms and the background *Figure 5*.

Then, the segments from the oil palm canopy from each GDSI were selected as training samples for each *Ganoderma* disease severity. The classifiers used in OBIA were SVM and KNN. The classification results of OBIA using SVM and KNN classifier are shown in *Figure 6*. The classification results classified oil palm canopies into four GDSI which are green (0), blue (1), yellow (2) and red (3). The classification outputs are in raster format. The OBIA was conducted on each of the generated images in *Table 5* which are: a) D-CR-SR 3; b) D-CR-SR 5; c) D-CR-SR 7; d) D-CR-FDSR 3; e) D-CR-FDSR 5 and f) D-CR-FDSR 7. The classification accuracy of OBIA for each image is shown in *Table 5*.

TABLE 3. THE ROOT MEAN SQUARE ERROR (RMSE) VALUES COMPARISON BETWEEN SPECTRORADIOMETER AND DENOISED HYPERSPECTRAL IMAGE

Section	1	2	3	4	5	6
A	-	0.026111233	0.009738559	0.008359466	0.006673	0.00563
B	0.032150344	0.009934903	0.006768957	0.006176466	0.005866852	-
C	-	0.013242752	0.010271097	0.00846282	0.00741182	

TABLE 4. THE BEST SIGNIFICANT WAVELENGTHS IDENTIFIED FROM DENOISED HYPERSPECTRAL IMAGE USING MRMR

Number of best significant wavelengths	D-CR-SR (nm)	Index	D-CR-FDSR (nm)	Index
3	749.69	0.3766	550.00	0.3943
	602.94	0.2759	650.00	0.3794
	922.76	0.0523	790.83	0.3172
5	749.69	0.3766	550.00	0.3943
	602.94	0.2759	650.00	0.3794
	922.76	0.0523	790.00	0.3172
	411.61	0.0374	662.00	0.2204
	490.94	0.0368	889.40	0.2125
7	749.69	0.3766	550.00	0.3943
	602.94	0.2759	650.00	0.3794
	922.76	0.0523	790.00	0.3172
	411.61	0.0374	662.00	0.2204
	490.94	0.0368	889.40	0.2125
	896.11	0.0366	601.00	0.1121
	803.88	0.0362	908.00	0.1098

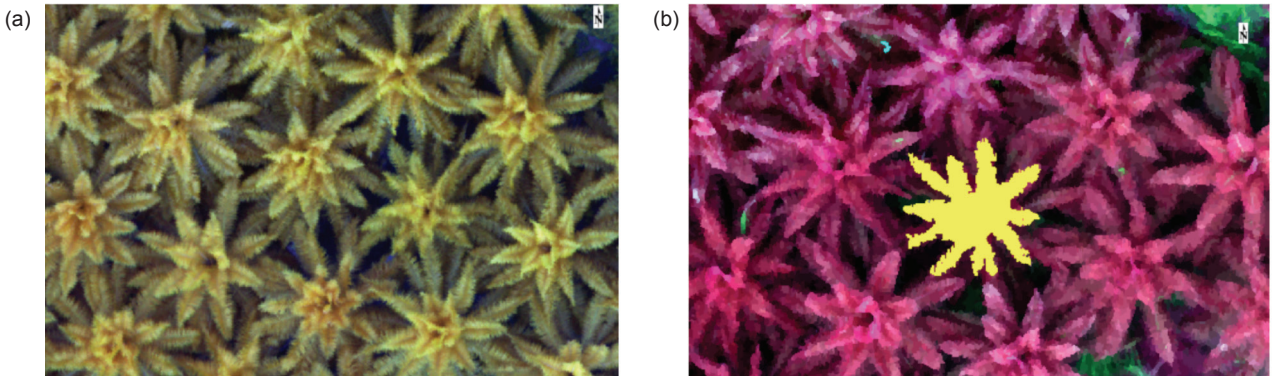

Figure 5. Outputs of the segmentation process: (a) Original image, and (b) segmented image of the oil palm canopy from the hyperspectral image.

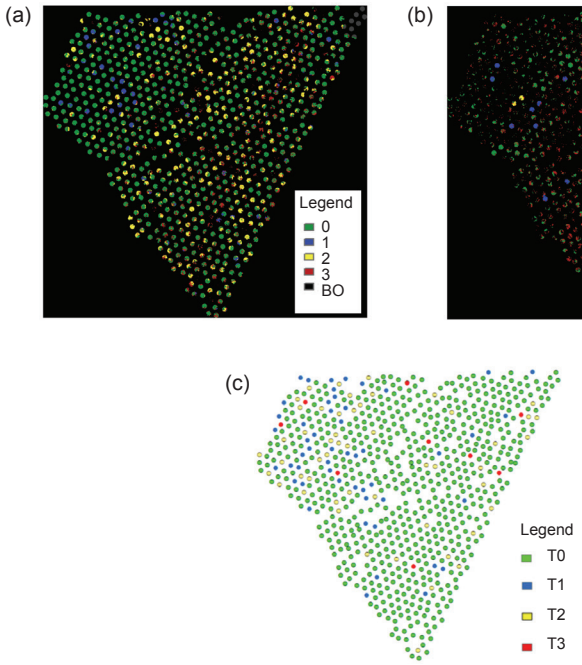

Figure 6. The OBIA classification output image using (a) SVM and (b) KNN classifiers for D-CR-FDSR3 image. Green (healthy), blue (early/mild), yellow (moderate) and red (severe) degree of Ganoderma *infection in oil palm, and (c) ground census map.*

TABLE 5. THE OUTPUT IMAGES OF CLASSIFICATION USING OBIA WITH SVM FOR D-CR-SR AND D-CR-FDSR FOR THE 3, 5 AND 7 BEST SIGNIFICANT WAVELENGTHS

Image	Accuracy (%)		Overall accuracy (%)	Image	Accuracy (%)		Overall accuracy
D-CR-SR 3	T0	90	60.00	D-CR-FDSR 3	T0	95	92.50
	T1	20			T1	85	
	T2	30			T2	90	
	T3	100			T3	100	
D-CR-SR 5	T0	98	83.25	D-CR-FDSR 5	T0	60	71.25
	T1	60			T1	50	
	T2	75			T2	75	
	T3	100			T3	100	
D-CR-SR 7	T0	30	40.00	D-CR-FDSR 7	T0	70	70.00
	T1	0			T1	50	
	T2	30			T2	60	
	T3	100			T3	100	

From the classification results in *Table 5*, the best classifier is SVM as compared to KNN. The best dataset for the SVM Classifier is the D-CR-FDSR 3 and D-CR-SR 5 with overall accuracy of 92.50% and 83.25%, but D-CR-SR 5B shows low accuracy for T1 classification. Meanwhile, D-CR-FDSR 3 provides good accuracy for T1 classification (85.00%) and very good classification accuracy for T0, T2 and T3. The results have shown that the integration of image segmentation with classifiers can enhance the capability of hyperspectral images for the detection of early infection of *Ganoderma* in oil palm.

Our study has successfully developed a new method for hyperspectral image processing, which requires a 2-step image pre-processing that involves continuum-removal and is followed by denoising using field spectral signatures as the benchmark, then OBIA to integrate the morphology of oil palm canopy with the significant spectral responses from the best wavelengths. Our approach manages to enhance the classification accuracy of each GDSI. Our study also suggested that the SVM classifier performed far better than KNN in the OBIA based on the comparison of the classification raster image with the ground census map in *Figure 6*. Our study also identified the seven most significant wavelengths from the MRMR technique which are 550.00, 650.00, 790.00, 662.00, 745.38, 704.59 and 501.21 nm. We then compared the position of our significant wavelengths with the other five studies as shown in *Figure 7*.

Figure 7 shows significant wavelength positions for the detection of *Ganoderma* BSR disease in oil palm from five previous studies and compared them with our findings. *Figure 7* shows that the significant wavelengths are located between 500 to below 1,000 nm. Most of the wavelengths are located at an overlap between 500-550 and 650-800 nm. This region has been reported to have a significant correlation with chlorophyll content changes, stomatal conductance and other photosynthesis-related parameters. There is a limited number of studies that have been conducted using hyperspectral images from drones for *Ganoderma* BSR disease detection in oil palm (Kurihara *et al.*, 2022). Our results agreed with the findings by Kurihara *et al*. (2022) that identified wavelengths of 560, 690, 710, 730 and 750 nm are suitable to be used in spectral indices generated from hyperspectral images from drones for *Ganoderma* BSR disease detection in oil palm. These regions must be explored in depth to identify what physiological changes in the oil palm foliar caused the subtle changes in the spectral responses when infected with *Ganoderma*. The significant wavelengths identified from our studies have a very good correlation with the significant wavelength regions suggested by Azmi *et al*. (2020) and Nisfariza (2012) except for the 800 nm and above spectral region.

These results concurred with the study conducted by Azmi *et al*. (2020) where they used a FireflEYE S185 (Cubert GmbH, Ulm, Germany) snapshot camera with wavelengths ranging from 450 to 950 nm (125 bands) covering the visible (blue, green, and red) and near-infrared (NIR) regions with a sampling interval of 4.0 nm was used. They used 28 seedlings of DxP where 15 seedlings were inoculated with the *Ganoderma* pathogen. The image acquisition was conducted five months after transplanting. The camera was mounted horizontally on a custom tripod and was positioned 2.6 m from the ground consisting of eight-month oil palm seedlings from healthy and *Ganoderma*-infected oil palms. They suggested that significant wavelengths from the NIR band have the capability to 100% discriminate between healthy and *Ganoderma*-infected oil palms.

On the contrary, other studies that used ground-based hyperspectral sensors suggested that only NIR played the most significant role in discriminating between healthy and other *Ganoderma* infection severity (Izzuddin *et al.*, 2010;

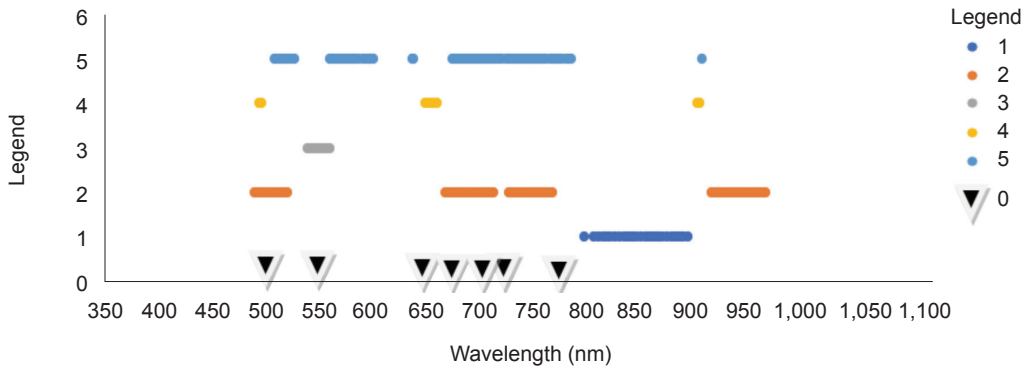

Figure 7. Position of significant wavelengths for detection of Ganoderma *disease in oil palm from five existing studies: 0) Significant wavelengths from CR-SG-FDSR-3B; 1) Azmi* et al. *(2020); 2) Lelong* et al. *(2010); 3) Ahmadi* et al. *(2017); 4) Izzuddin (2010) and 5) Nisfariza (2012).*

2017; 2018; Khairunniza-Bejo *et al.,* 2021; Nisfariza, 2012). The contradiction between the ground-based hyperspectral studies with our drone-based hyperspectral studies was due to the difference in samples. The ground-based hyperspectral studies used seedlings and immature oil palms in a controlled environment such as oil palm nurseries and glass houses meanwhile our study took samples from mature oil palms in the field. The morphology and physiology of immature and young oil palms are different.

These physiological changes in the oil palm foliar between healthy and *Ganoderma*-infected or other are likely stresses in oil palm also reported by several ground and lab-based studies (Haniff *et al.,* 2005; Putranto, 2018; Wei *et al.,* 2021). These physiological changes in the oil palm foliar also cause changes to the spectral properties of the oil palm canopy. Putranto (2018) agreed with Hanif *et al.* (2005) on the suggestion that water stress in oil palm causes a decrease in stomatal conductance.

Wei *et al. (*2021) also mentioned that abiotic stress due to inefficient water intake from pathogen infection affects the physiology of the oil palm. The abiotic stress decreased chlorophyll content, variable fluorescence (Fv), maximum fluorescence (Fm), variable fluorescence and maximum fluorescence ratio (Fv/Fm) of oil palm leaves, whereas initial fluorescence (F0) and non-photochemical quenching coefficient (NPQ) increased, indicating that the plants were affected by water stress.

These studies supported the fact that disruption to the root of the plant, including oil palm can affect the physiology traits in the foliar. These changes can be asymptomatic and can be measured using spectral signatures from hyperspectral remote sensing imagery. Finally, our findings showed that hyperspectral cameras are useful for conducting a thorough diagnosis via spectral responses from plants for disease detection. The results from the diagnosis provide a set of several narrow wavelengths that are specific for GDSI classification. Our results could open opportunities to develop a new camera that is specific for *Ganoderma* detection in oil palm and can reduce the cost of drone operation in the field. Our findings also confirmed that hyperspectral images provide higher accuracy as compared to multispectral images for the detection of *Ganoderma* infection in oil palms (Izzuddin *et al.,* 2020).

CONCLUSION

In this study, the hyperspectral image from the drone was accessed using CR and denoised using the S-G technique before conducting OBIA methods that integrate segmentation and merging with SVM and KNN classifiers to categorise oil palm into four GDSI namely T0, T1, T2 and T3. The results showed different performances of each band and different band combinations in the classification of the disease severity categories. Nevertheless, the combinations of three, five and seven bands' images of the FDSR had shown good results (70.0%-92.5%). This study showed that the three-band combination of D-CR-FDSR image analysed using OBIA analysis can detect early, moderate, and severe infection of *Ganoderma* disease in oil palm. For future work, extensive experiments of OBIA analysis with deep learning should be conducted to enhance the detection of early infection of *Ganoderma* in oil palm using multispectral band combinations. Specific cameras for drones could also be developed for *Ganoderma* detection in oil palm using the new set of significant wavelengths, thus reducing the cost of operation in the field.

ACKNOWLEDGEMENT

We would like to thank the Director-General of MPOB for permission to publish this article and the staff of Agronomy and Geospatial Technology (AGT) and Plant Protection and Biosecurity (PPB) Unit, MPOB for their support and commitment to this study.

REFERENCES

Azmi, A. N. N., Bejo, S. K., Jahari, M., Muharam, F. M., Yule, I., & Husin, N. A. (2020). Early detection of *Ganoderma boninense* in oil palm seedlings using support vector machines. *Remote Sensing*, *12*(23), 3920. https://doi.org/10.3390/rs12233920

Basiron, Y. (2007). Palm oil production through sustainable plantations. *European Journal of Lipid Science and Technology*, *109*(4), 289–295. https://doi.org/10.1002/ejlt.200600223

Cortes, C., & Vapnik, V. (1995). Support-vector networks. *Machine learning*, *20*(3), 273–297. https://doi.org/10.1007/bf00994018

Gholami, R., & Fakhari, N. (2017). Support vector machine: Principles, parameters, and applications. In *Machine learning* (pp. 515–535). https://doi.org/10.1016/b978-0-12-811318-9.00027-2

Haniff, M. H., Ismail, S., & Idris, A. S. (2005). Gas exchange responses of oil palm to *Ganoderma boninense* infection. *Asian Journal of Plant Sciences, 4*(4), 438–444. https://doi.org/10.3923/ajps.2005.438.444

Idris, A. S., & Rafidah, A. R. (2008). Polyclonal antibody for detection of *Ganoderma*. *MPOB Information Series*, *No. 405*, 1–4.

Idris, A. S., Kushairi, D., Ariffin, D., & Basri, M. W. (2006). Technique for inoculation of oil palm germinated seed with *Ganoderma*. *MPOB Information Series*, *314*, 1–4.

Idris, A. S., Kushairi, D., Ismail, S., & Ariffin, D. (2004). Selection for partial resistance in oil palm progenies to *Ganoderma* basal stem rot. *Journal of Oil Palm Research*, *16*, 12–18.

Idris, A. S., Mazliham, M. S., Loonis, P., & Basri, M. W. (2010). *GanoSken* for early detection of *Ganoderma* infection in oil palm. *MPOB Information Series*, *442,* 1–3.

Idris, A. S., Nur-Rashyeda, R., Hefni, R. M., Shamala, S., & Norman, K. (2016). *Standard operating procedures (sop) guidelines for managing* Ganoderma *disease in oil palm*. MPOB.

Izzuddin, M. A. (2010). *Early detection of* Ganoderma *disease in oil palm* (Elaeis guineensis *Jacq*.) *using field spectroscopy*. [Master's thesis]. Universiti Putra Malaysia.

Izzuddin, M. A., Hamzah, A., Nisfariza, M. N., & Idris, A. S. (2020). Analysis of multispectral imagery from unmanned aerial vehicle (UAV) using object-based image analysis for detection of *Ganoderma* disease in oil palm. *Journal of Oil Palm Research*, *32*(3), 497–508. https://doi.org/10.21894/jopr.2020.0035.

Izzudin, M. A., Idris, A. S., Wahid, O., Nishfariza, M. N., & Shafri, H. Z. M. (2013). Field spectroscopy for detection of *Ganoderma* disease in oil palm. *MPOB Information Series, 532*, 1–4.

Izzuddin, M. A., Nisfariza, M. N., Ezzati, B., Idris, A. S., Steven, M. D., & Boyd, D. (2018). Analysis of airborne hyperspectral image using vegetation indices, red edge position and continuum removal for detection of *Ganoderma* disease in oil palm. *Journal of Oil Palm Research*, *30*(3), 416–428. https://doi.org/10.21894/jopr.2018.0037

Kurihara, J., Koo, V. C., Guey, C. W., Lee, Y. P., & Abidin, H. (2022). Early detection of basal stem rot disease in oil palm tree using unmanned aerial vehicle-based hyperspectral imaging. *Remote Sensing*, *14*(3), 799. https://doi.org/10.3390/rs14030799

Lan, Y., Huang, Z., Deng, X., Zhu, Z., Huang, H., Zheng, Z., Lian, B., Zeng, G., & Tong, Z. (2020). Comparison of machine learning methods for citrus greening detection on UAV multispectral images. *Computers and Electronics in Agriculture*, *171*, 105234. https://doi.org/10.1016/j.compag.2020.105234

Liang, J. (2017). *Spectral-spatial feature extraction for hyperspectral image classification*. [Ph.D thesis]. Australian National University.

Mazliham, M. S., Loonis, P., & Idris, A. S. (2006). Mass function initialization rules for *Ganoderma* infection detection by tomography sensor. *Proceeding of the 2nd IASTED International Conference on Computational Intelligence, CI 2006,* 377–386.

Nisfariza, M. N. (2012). *Early detection of* Ganoderma *basal stem rot disease of oil palm by hyperspectral remote sensing.* [Ph.D thesis]. University of Nottingham.

Putranto, D. (2018). *Stomatal conductance and chlorophyll fluorescence of oil palm under field conditions*. Wageningen University.

Roslan, A., & Idris, A. S. (2012). Economic impact of *Ganoderma* incidence on Malaysian oil palm plantation – A case study in Johor. *Oil Palm Industry Economic Journal*, *12*(1), 24–30.

Ruffin, C., King, R. L., & Younan, N. H. (2008). A combined derivative spectroscopy and Savitzky-Golay filtering method for the analysis of hyperspectral data. *GIScience & Remote Sensing*, *45*(1), 1–15. https://doi.org/10.2747/1548-1603.45.1.1

Shafri, H. Z. M., Anuar, M. I., Seman, I. A., & Noor, N. M. (2011). Spectral discrimination of healthy and *Ganoderma*-infected oil palms from hyperspectral data. *International Journal of Remote Sensing*, *32*(22), 7111–7129. https://doi.org/10.1080/01431161.2010.519003

Singh, G. (1991). *Ganoderma* – The scourge of oil palm in the coastal area. *Proceding of* Ganoderma *Workshop.* (pp. 7-35). PORIM.

Wei, L., Martin, J. J. J., Zhang, H., Zhang, R., & Cao, H. (2021). Problems and prospects of improving abiotic stress tolerance and pathogen resistance of oil palm. *Plants*, *10*(12), 2622. https://doi.org/10.3390/plants10122622